Preprints of the 21st IFAC World Congress (Virtual)
Berlin, Germany, July 12-17, 2020

LIDAR-based Gust Alleviation Control System: Obtained Results and Flight Demonstration Plan

Yoshiro Hamada * **Ryota Kikuchi** * **Hamaki Inokuchi** *

* *Japan Aerospace Exploration Agency (JAXA), Tokyo, Japan (e-mail: {hamada.yoshiro},{kikuchi.ryohta},{inokuchi.hamaki}@jaxa.jp)*

Abstract: This paper presents a flight demonstration project for LIDAR-based gust alleviation control currently planned in Japan. The onboard coherent Doppler LIDAR has already been developed and validated by flight experiments. The wind velocity estimation algorithm has also been developed which can estimate two-dimensional distribution of wind field between two laser beams of the LIDAR system. These components are to be combined with the preview control law which utilizes the estimated wind velocities in front of the aircraft, and to be proven in the flight demonstration. This paper shows the results obtained so far and introduces the flight demonstration under planning.

Keywords: Aircraft control, Gust alleviation, LIDAR, Preview control

1. INTRODUCTION

The number of serious incidents of mid-large sized aircraft in Japan is more than 40 from 2001 through 2014, and about half of these incidents are due to wind gust (Japan Transport Safety Board (2015)). According to NTSB report, there were 18 U.S. air carrier accidents caused by air turbulence in 2003, which is more than three times as many as in 1980 (Federal Aviation Administration (2006)). Not only in Japan and the U.S., but globally the number of turbulence accidents of aircraft has increased and should be reduced for improving aviation safety.

Currently most civil aircrafts have onboard weather RADAR (RAdio Detection And Ranging), which can detect areas of clouds causing turbulence. Although this equipment is useful to some extent, it cannot detect clear air turbulence (CAT), which occurs suddenly even in the absence of clouds, and therefore it is not sufficient for preventing turbulence accidents. In contrast, JAXA (Japan Aerospace eXploration Agency) has developed an onboard Doppler LIDAR (LIght Detection And Ranging) system, which can detect not only CAT but windshear, downbursts, wake-vortex and mountain wave in clear air conditions at a range of about 10 km ahead of an aircraft. The LIDAR system has been validated by flight experiments using a business jet aircraft and a wide-body transport aircraft (Inokuchi et al. (2018); Inokuchi and Akiyama (2019)). In these experiments, an onboard turbulence information system that provides turbulence information to pilots based on LIDAR measurements has also been demonstrated and proven to be effective as a warning system (Matayoshi et al. (2018)).

Although the LIDAR-based onboard turbulence information system is useful, it is difficult to avoid turbulence in high altitude since the detection range is too short to warn pilots. In order to prevent accidents due to turbulence, it is important not only to provide turbulence information to pilots but also to alleviate violent aircraft motion by automatic control. This type of automatic control technology is called the "gust (load) alleviation control" and has been studied since the 1970s (Regan and Jutte (2012)). Most of them were based on only feedback sensors such as IMUs, but recently there have been some studies which take advantage of LIDAR measurement data (Sato (2010); Fezans and Joos (2017)). JAXA has also been conducting researches on gust alleviation control using the LIDAR system (Hamada (2013)). In these studies, onboard LIDAR technology, real-time airflow vector estimation method and control law which utilizes estimated wind velocities are of importance.

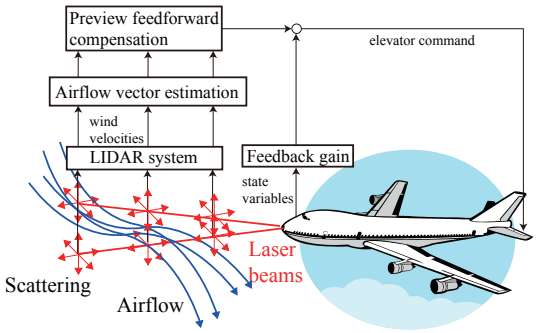

Fig. 1. Basic concept of the LIDAR-based gust alleviation control system.

This paper presents JAXA's ongoing research project on the LIDAR-based gust alleviation control, STABLE (System for Turbulence Alleviation By Lidar Employed controller). The gust alleviation system that will be demonstrated in STABLE is composed of mainly aforementioned three components. The onboard coherent Doppler LIDAR has been developed and flight demonstration has been carried out to show its effectiveness. The real-time airflow

vector estimation algorithm and gust alleviation control law have also been developed, and proven by some numerical simulations. This paper presents these obtained results so far and introduces the flight demonstration plan.

2. OVERVIEW OF THE GUST ALLEVIATION CONTROL SYSTEM

Figure 1 shows the basic concept of the LIDAR-based gust alleviation control system to be demonstrated in STABLE project. The LIDAR emits two laser beams and measures wind velocities along these beams. The estimation algorithm calculates a two-dimensional distribution of wind field between the two laser beams in real time based on the LIDAR measurement data. The gust alleviation control law is designed as a so-called "preview control", which is composed of a conventional feedback law using the IMU measurement data and a preview feedforward compensation using the outputs from the estimation algorithm. Each component is described in the following sections.

3. ONBOARD DOPPLER LIDAR SYSTEM

The basic specifications of the developed coherent Doppler LIDAR system are shown in Table 1. The antenna has two telescopes: a 150 mm aperture telescope for long range observation and a 50 mm aperture telescope for vector conversion of short range wind speeds. Emitted laser light is scattered by fine aerosol particles in the atmosphere, and back-scattered light is condensed by the telescopes and received by the optical transceiver. Since the wavelength of the received light varies according to the velocity of the aerosol particles due to the Doppler effect, wind speed can be calculated by comparing the wavelength of the transmitted light with the received light. By "binning" received signals along the time axis, it is possible to obtain wind speeds simultaneously at multiple observation ranges. Signal processing and system management are performed by the signal processor unit, which is a commercial off-the-shelf general-purpose computer.

The LIDAR system was evaluated in a series of 19 flights by a Gulfstream II over the land and sea around the Chubu area of central Japan between December 17, 2016 and February 10, 2017. Figure 2 shows the overview of the experimental system. The optical antenna was installed in a pod mounted on the aircraft's lower fuselage so that the laser beam was emitted in the forward direction. A double wedge prism-type beam direction controller for steering the laser beam was installed in front of the optical antenna apparatus so that the beam direction could be adjusted from the cabin and matched with the flight direction. All other system components were installed in the cabin. In this flight test campaign, the LIDAR was used as a one-axis LIDAR system, that is, only the larger telescope for long range observation was used.

Table 1. Specifications of the LIDAR system.

Laser wavelength	1.55 μm
Laser output	3.3 W
Pulse repetition frequency	1000 Hz
Laser beam diameter	150 mm / 50 mm
System weight	83.7 kg
Power consumption	936 W

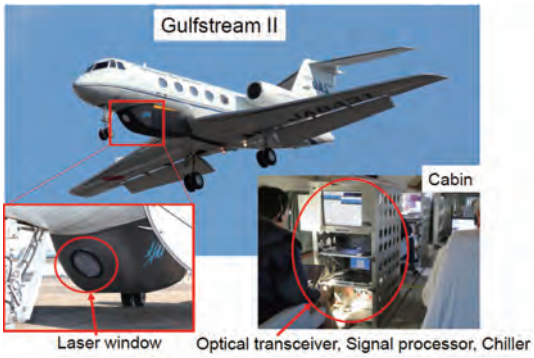

Fig. 2. Overview of the experimental system for the developed Doppler LIDAR.

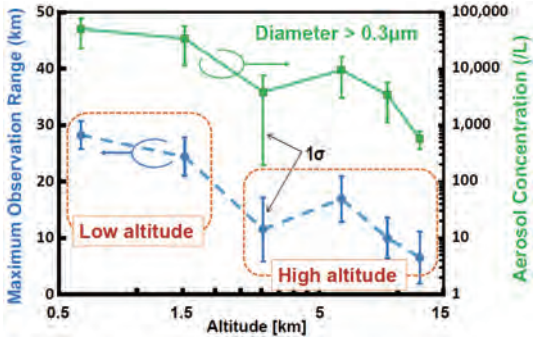

Fig. 3. Maximum observation range and aerosol concentration through the flight experiments.

The maximum observation range and aerosol number concentration measured at each altitude are shown in Fig. 3. Since the variation among observations was large, observations were made 7 to 10 times. Average values are plotted and standard deviations are shown by error bars. The dashed blue line indicates the maximum observation range of the wind speed observed by the LIDAR. The solid green line indicates the concentration of aerosol particles whose diameter is 0.3 μm or larger. The concentration was measured by an optical particle counter with air sampled from an isokinetic flow as described in Wilcox (1956). Generally, as altitude increases, the aerosol concentration decreases and the maximum observation range tends to decrease accordingly. However, in these experiments the observation range was particularly low near the altitude of 3 km. This reason is presumed to be weather related since the aerosol concentration also decreases in the same way. These results indicate that the observation range at low altitudes below 1.5km exceeds 20km, but at high altitudes above 3km, the average observation range is about 10 km. Since the range of 10km only gives a warning of several tens of seconds before encountering turbulence, it is too short to warn pilots and to avoid turbulence. For this reason, this study uses gust alleviation control instead of providing turbulence information to pilots at high altitudes.

The accuracy of the measured wind velocity was also evaluated in the flight tests. Since the LIDAR can measure true airspeed (TAS), it was compared with the value of TAS computed from Pitot tube measurements and the TAS estimated by the speed-course method under the calm air conditions. The measurements were carried out at altitudes of 0.6 km, 1.5 km, 3 km, 6 km, 9 km and 12

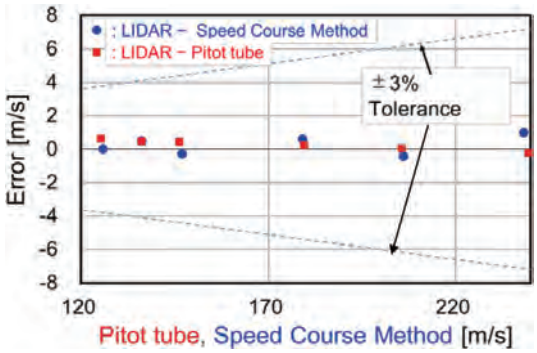

Fig. 4. Differences between measured TAS by LIDAR and measured TAS by other methods.

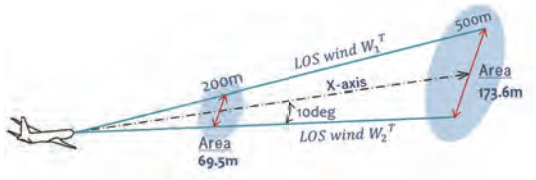

Fig. 5. Outline of the two-axis Doppler LIDAR system.

km. The results were shown in Fig. 4, where the red dots indicate the differences between LIDAR measurement and Pitot tube measurement, and the blue dots indicate the difference between LIDAR measurements and estimated values by the speed-course method for each altitude. The dashed line shows the tolerance of the airspeed sensor specified in the airworthiness standard. In these flight tests, the bias was 0.28 m/s and the standard deviation was 0.32 m/s when compared with the Pitot tube, and the bias was 0.25 m/s and the standard deviation was 0.55 m/s when compared with the speed-course method. These results indicate that the measurement accuracy of the LIDAR is comparable to that of the Pitot tube.

Although these results were, as mentioned above, obtained by the one-axis (long range) LIDAR system, the two-axis (short range) LIDAR system was also developed and validated by flight tests. The two-axis LIDAR system is expected to achieve the maximum observation range of about 600 m, the measurement frequency of 5 Hz and the wind velocity measurement accuracy of the same level as the one-axis LIDAR system. Since the one-axis Doppler LIDAR system can only measure the line-of-sight (LOS) wind velocity, the two-axis Doppler LIDAR system is necessary to estimate vertical wind velocity and use the estimated value for the preview control law.

4. REAL-TIME AIRFLOW VECTOR ESTIMATION

It is crucial to estimate vertical wind velocities with high accuracy for the LIDAR-based gust alleviation control system since the vertical velocity has the greatest influence on the local lift through the change of the angle of attack. The vertical wind velocities can be reconstructed from the differences between the upward and downward LOS winds. Figure 5 shows the outline of the two-axis Doppler LIDAR system. The angle between the airplane's X-axis and the LOS is 10 deg for each upward/downward laser beam. The LIDAR measures wind velocities along each LOS, which are used to estimate vertical and horizontal wind velocities in the triangular area between the laser beams.

In the most conventional way, the airflow vector in the triangular area between two laser beams can be estimated by a simple vector conversion:

$$u_g^T = \frac{(W_1^T + W_2^T)}{2\cos\theta} \tag{1}$$

$$w_g^T = \frac{(W_1^T - W_2^T)}{2\sin\theta} \tag{2}$$

where u_g^T and w_g^T are horizontal and vertical velocity components, W_1^T and W_2^T are LOS wind velocities along upward and downward beams, and θ is the angle between X-axis and each laser beam, which is 10 deg in this paper. It should be noted that this method assumes uniformity of the airflow in the triangular area. This assumption depends on atmospheric conditions encountered by the aircraft and does not hold in a real situation such as a fully turbulent field with atmospheric turbulence and gust. In addition, when the estimated wind position is far ahead from the aircraft, the distance between two laser beams becomes too large to assume uniformity. For example, the distance between two laser beams is 173.6 m at LOS distance of 500 m.

In order to estimate airflow vector with high accuracy in a real flight condition, a new estimation algorithm is proposed (Kikuchi (2017)). While the simple vector conversion utilizes only the current LOS wind data, the algorithm stores the LOS wind data in each measurement step and uses the stored data with the current LOS wind data. Figure 6 shows the overview of the proposed estimation method when an actual data point and two-past LOS wind data points are used. The current and stored data are used to extrapolate the vertical and horizontal wind velocities in the triangular area of Fig. 6, and the area between the two laser beams has not been measured directly by the LIDAR. Suppose the aircraft speed is V and the time span of observation is dt, then the airflow moves $V \times dt$ backward because the aircraft is advancing. The actual observation time is denoted as T and past observation times are $T-1$ and $T-2$. The proposed method uses the actual LOS wind values (W_1^T and W_2^T) and the past LOS wind values (W_1^{T-1}, W_2^{T-1} and W_1^{T-2}, W_2^{T-2}). The distances between the horizontal line and each laser beam are denoted as z^T, z^{T-1} and z^{T-2}, respectively. A first-degree polynomial expression of the least-squares method (LSM) is applied and using some LOS wind data values, the wind field values are extrapolated according to the following equations.

$$W_j'(z) = a_j z + b_j, \quad \text{for } j = 1, 2, \tag{3}$$

$$a_j = \frac{N\sum_{i=T_N}^{T} z^i W_j^i - \sum_{T_N}^{T} z^i \sum_{T_N}^{T} W_j^i}{N\sum_{i=T_N}^{T}(z^i)^2 - (\sum_{i=T_N}^{T} z^i)^2},$$

$$b_j = \frac{\sum_{i=T_N}^{T} z^i \sum_{i=T_N}^{T} W_j^i - \sum_{T_N}^{T} z^i W_j^i \sum_{T_N}^{T} z^i}{N\sum_{i=T_N}^{T}(z^i)^2 - (\sum_{i=T_N}^{T} z^i)^2},$$

where N denotes the number of the LOS wind values used for estimation of $W_j'(z)$, $T_N = T - (N-1)$ and $W_j'(z)$ is the LOS wind value at z from the horizontal line. The

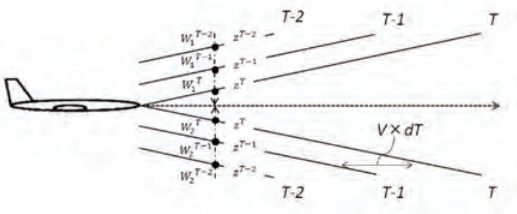

Fig. 6. Overview of the proposed estimation method. The current and stored (two-past) LOS wind data are used here.

calculated polynomial expression is used to obtain the extrapolated LOS wind at the horizontal line, and the airflow vector is calculated by simple vector conversion using the extrapolated LOS wind values. Although the simple vector conversion only can be applied to homogenous wind field conditions, the proposed algorithm can extrapolate data points by using past measurements so that it can be used in non-homogenous wind field conditions. Consequently, unlike the simple vector conversion, the proposed method can estimate a two-dimensional "distribution" of wind field between the two laser beams.

As for the measurement error, two filtering algorithms are used in this study to remove the error and the loss of data of LIDAR measurements. Firstly, a filtering algorithm that is a simple representation of the Kalman filter with simplified Kalman gain (Misaka et al. (2015)) is used. The algorithm assumes that infinite variance is used to exclude outliers and loss of data. It uses the LIDAR spectrum data at each range-bin and defines the validity of the measurements during the LIDAR data peak detection process. Secondly, a robust LSM estimation, based on Tuckey ' s biweight methodology (Huber and Ronchetti (2008)), is carried out to reduce the impact of the error in the LOS wind velocity. Unlike the first method, which used the spectrum data from LIDAR observations, this method is based on LOS wind data. Although the filtering algorithm based on a simple Kalman filter can remove the error, it is essential to deal with the error and the loss of data of the LIDAR more carefully when the filtering algorithm is used for the preview control. Thus the robustness of the estimated airflow vector is secured by using the filtering algorithm based on a simple Kalman filter together with robust LSM. In addition, the robust LSM estimation can make use of the extrapolation algorithm effectively. Therefore, the robust LSM estimation provides a simpler and more robust algorithm. The concept of a robust LSM is proven by analyzing the difference between the observed LOS wind values and those LOS wind values estimated by the polynomial expression.

The numerical simulations were carried out to confirm the accuracy of the estimated airflow vector. The ideal vortex model is defined as in Hinton and Tatnall (1997) and used in order to generate a reference wind field for the simulations. A large amount of emulated LIDAR measurements along flight paths is generated from the wind filed. Then the airflow vector is estimated using the emulated LIDAR measurement data and the estimated airflow vector is compare with the reference field of the ideal vortex model. Figure 7 shows the distribution of vertical wind velocity generated by Hallock-Burnham vortex model.

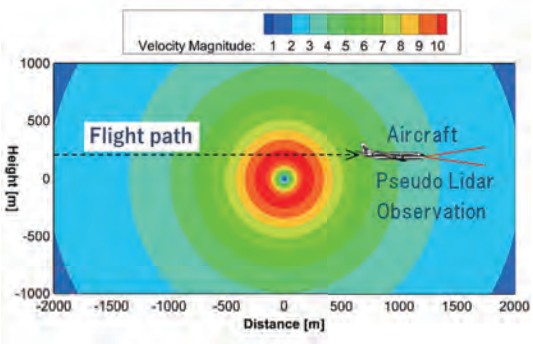

Fig. 7. Distribution of vertical wind velocity generated by the vortex model.

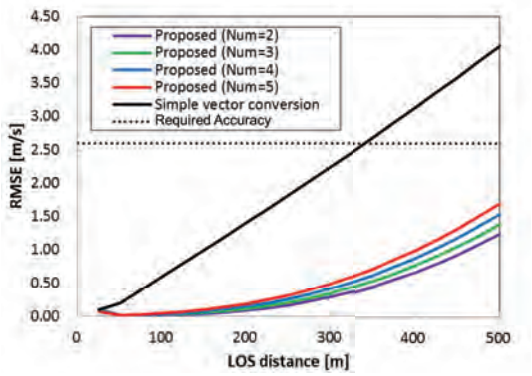

Fig. 8. Statistical accuracy of estimated vertical wind velocities.

Figure 8 shows the statistical accuracy of estimated vertical wind velocities evaluated by 100-pseudo flight paths. In the legend "Num" means the number of stored data used in the extrapolation. Results of different "Num"s are compared in the figure. The dotted line is the required accuracy for the gust alleviation control law. The results show that the simple vector conversion can not satisfy the requirement at LOS distance farther than 350 m. This means that it is difficult to use the simple vector conversion for gust alleviation preview control. On the other hand, the proposed method is able to satisfy the requirement for each "Num"s. In this case, lower Num leads to better estimation accuracy. In an vortex model such as this example, the accuracy was reduced by increasing "Num" because the distant data cannot be represented by the linear approximation of (3). On the other hand, increasing "Num" ensures robustness against outliers, so "Num" should be determined by taking the balance between accuracy and robustness into consideration. In conclusion, the proposed method can estimate vertical wind velocity with higher accuracy than the simple vector conversion.

5. GUST ALLEVIATION PREVIEW CONTROL

As mentioned in Section 2, the control system is designed as a preview control law, which is composed of a conventional feedback control and a preview feedforward compensation. Preview control is a control methodology that takes advantage of prior information regarding imminent disturbances or commands (Sheridan (1966)). An estimated wind velocity, obtained from the estimation algorithm, ahead of the current aircraft position can be regarded as

a velocity ahead of the current time step. For example, the future vertical gust velocity $w_g(k+h)$ is measured as the vertical gust velocity at $h \times \Delta t \times V$ [m] ahead of the current aircraft position, where Δt is the sampling time and V is the airspeed of the aircraft [1]. Thus the preview control technique is available using the LIDAR system. In addition, it should be noted that, unlike other LIDARs, the LIDAR referred to Inokuchi and Akiyama (2019) can simultaneously measure the vertical wind velocities in multiple range segments in real time. This means that the preview controller can utilize not only a single future velocity $w_g(k+h)$ but a *series* of future velocities $w_g(k), w_g(k+1), \ldots, w_g(k+h)$.

The aim of the gust alleviation here is to prevent in-flight accidents resulting from sudden unexpected wind gusts. A sudden change of vertical wind speed may cause unsecured persons and even heavy objects to momentarily float up and then suddenly drop to the floor, potentially causing injuries. This type of wind gust is usually modeled as "discrete gusts", where the gust velocity varies in a deterministic manner (see Chapter 14 of Wright and Cooper (2007)). Thus, in the controller synthesis the controller is designed to minimize the magnitude of vertical acceleration against discrete gusts which are not modeled by spectral filters. For the performance index, the H_2 norm is appropriate for the controller's objective because $||H_{zw}||_2$ bounds the least upper bound of the absolute value of z when w has an energy bound (see Section 2.3 of Doyle et al. (1992)), which is true of discrete gusts.

This paper focuses only the longitudinal motions of the aircraft. The frequencies of the aircraft's vibration modes are here assumed to be far higher than the frequency of the short-period mode, and therefore the vibration modes are supposed not to be excited by gust alleviation control. Thus only the rigid mode model is considered below. A linearized aircraft mathematical model at a cruise flight condition can be described in the discrete-time state-space form:

$$\boldsymbol{x}(k+1) = A\boldsymbol{x}(k) + B_u\delta_{e_c}(k) + B_w w_g(k),$$

where $\boldsymbol{x}(k)$ is the state vector, $\delta_{e_c}(k)$ elevator command and $w_g(k)$ vertical gust velocity at time step k. In this case the elevator is the control input and the vertical gust is the disturbance input. The state vector is defined as

$$\boldsymbol{x}(k) := [u(k) \;\; w(k) \;\; q(k) \;\; \theta(k) \;\; \delta_e(k)]^T$$

where $u(k)$ is axial velocity, $w(k)$ vertical velocity, $q(k)$ pitch rate, $\theta(k)$ pitch angle and $\delta_e(k)$ elevator deflection around the equilibrium point. Since the actuator of the elevator is modeled as a first-order model in this case, $\delta_e(k)$ is included in $x(k)$. The vertical acceleration a_z is given by

$$a_z(k) = C\boldsymbol{x}(k) + D_u\delta_{e_c}(k) + D_w w_g(k).$$

The controlled output is described by

$$\boldsymbol{z}(k) = \begin{bmatrix} Q^{\frac{1}{2}} a_z(k) \\ R_e^{\frac{1}{2}} \delta_{e_c}(k) \end{bmatrix} = C_z\boldsymbol{x}(k) + D_{zu}\delta_{e_c}(k) \qquad (4)$$

so as to minimize the weighted quadratic sum of vertical acceleration $a_z(k)$ and elevator command $\delta_{e_c}(k)$.

Simulation results of the gust alleviation preview control are shown below. In the previous studies, Hamada (2019) for example, simulations in a homogenous wind field have been only dealt with, but here the results of simulations in a vortex wind field shown in Section 4 are provided. Figure 9 shows the vortex wind field used in the simulations. The dotted line shows the nominal flight path of the simulated aircraft. The aircraft is to fly the wind field between wind velocities of 9 m/s and 12 m/s. A mathematical model of a small jet aircraft [2] in the cruise condition is used to design a control system and conduct flight simulations.

The preview control law is designed using the LMI-based synthesis condition proposed in Hamada (2019). In this simulation, H_2 optimal state feedback controller was firstly designed so as to minimize the controlled output (4). Then the static preview feedforward compensation was designed using the same controlled output (4). The designed preview control law has the form:

$$\delta_{e_c}(k) = u_{fb}(k) + u_{ff}(k), \quad \text{where}$$

- $u_{fb}(k)$: Feedback control
$$u_{fb}(k) = K_{fb}\boldsymbol{x}(k)$$
- $u_{ff}(k)$: Preview feedforward compensation
$$u_{ff}(k) = K_{ff}\left[w_g(k), w_g(k+1), \ldots, w_g(k+h)\right]^T.$$

The sampling time of the discrete-time system is set to 0.1 sec and preview length h to 44 (that is 4.4 sec). In general, the longer h makes the control performance better. In this simulation the possible longest value is adopted for h by taking into account the measurement range of the LIDAR and the aircraft's cruising speed. The future wind velocities $w_g(k+i)$ used in $u_{ff}(k)$ $(i = 0, \ldots, h)$ are estimated in two ways: the conventional vector conversion (2) and the proposed method based on (3).

Figures 10–11 show simulation results. The dotted lines correspond to the open loop case (that is $\delta_{e_c}(k) = 0$), the dashed lines to the preview control with the conventional estimation method and the solid lines to the preview control with the proposed estimation method. As mentioned in Section 4, since the uniformity assumption no longer holds in a vortex wind field, the conventional method cannot estimate the airflow vector correctly. As a matter of fact, Fig. 10 (upper) shows that the vertical acceleration of the preview control with conventional estimation is worse than that of the open loop case. This indicates that the preview control does not work with the conventional estimation. On the other hand, the preview control with proposed estimation suppresses the acceleration well. These results show that the preview control can be applied to general non-homogenous wind fields by using the proposed airflow estimation method.

6. PLANNED FLIGHT DEMONSTRATION

Currently the LIDAR system is being modified to be smaller and lighter in order to fit small experimental

[1] Here it is assumed that the gust wind does not change drastically during h step. This holds when the preview time $h \times \Delta t$ is sufficiently short.

[2] Such mathematical models can be found in some research papers. Here the model was constructed with reference to Berger et al. (2017).

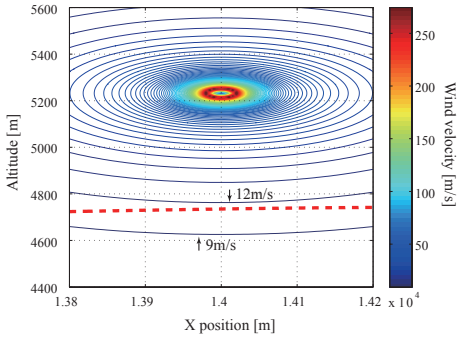

Fig. 9. Vortex wind field used in the simulations. The wind velocity on the same contour line is equal everywhere.

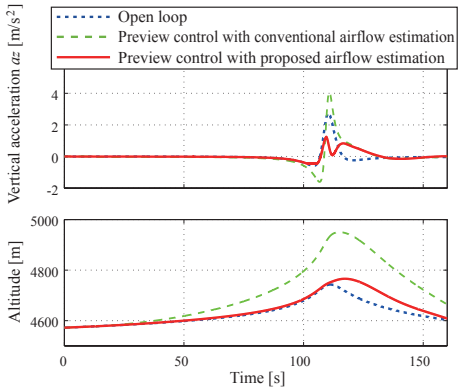

Fig. 10. Time histories of vertical acceleration and altitude for each case.

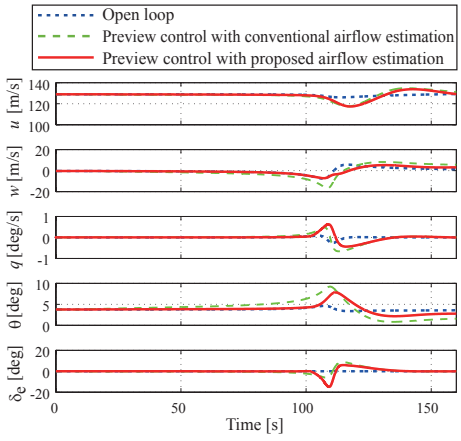

Fig. 11. Time histories of longitudinal states for each case.

aircrafts. Flight demonstrations are to be carried out in 2021 and 2022. In the first demonstration, the effectiveness of the LIDAR system and the estimation algorithm will be demonstrated without the gust alleviation preview control. In the second demonstration, the full LIDAR-based gust alleviation control system is to be installed to a Fly-By-Wire experimental aircraft and flight test campaign will be carried out. An experimental aircraft to be used in the flight demonstrations will be selected in the near future.

7. CONCLUSION

This paper presented the obtained results concerning LIDAR-based gust alleviation control and planned flight demonstration for it. The onboard LIDAR system and real-time airflow vector estimation will be demonstrated through flight experiments in 2021. After that, the whole gust alleviation system including preview control will be demonstrated in 2022. The results of these flight experiments will be presented in future conferences.

REFERENCES

Berger, T., Tischler, M., Hagerott, S.G., Cotting, M.C., Gray, W.R., Gresham, J., George, J., Krogh, K., D'Argenio, A., and Howland, J. (2017). Development and validation of a flight-identified full-envelope business jet simulation model using a stitching architecture. In *AIAA Modeling and Simulation Technologies Conference*, AIAA 2017–1550.

Doyle, J.C., Francis, B.A., and Tannenbaum, A.R. (1992). *Feedback Control Theory*. Macmillan Publishing Company, 866 Third Avenue, New York, New York 10022, the United States.

Federal Aviation Administration (2006). Preventing injuries caused by turbulence. *Federal Aviation Administration*, AC 120-88A.

Fezans, N. and Joos, H.D. (2017). Combined feedback and lidar-based feedforward active load alleviation. In *AIAA Atmospheric Flight Mechanics Conference*, AIAA 2017–3548.

Hamada, Y. (2013). Aircraft gust alleviation using discrete-time preview controller with prior gust information. In *Proceedings of the SICE Annual Conference 2013*.

Hamada, Y. (2019). New lmi-based conditions for preview feedforward synthesis. *Control Engineering Practice*, 90, 19–26.

Hinton, D.A. and Tatnall, C.R. (1997). A candidate wake vortex strength definition for application to the nasa aircraft vortex spacing system (avoss). *NASA Technical Reports*, NASA-TM-110343.

Huber, P.J. and Ronchetti, E.M. (2008). *Robust Statistics*. Wiley.

Inokuchi, H. and Akiyama, T. (2019). True airspeed measured by an airborne coherent doppler lidar. In *Proceedings of the Asia-Pacific International Symposium on Aerospace Technology*.

Inokuchi, H., Akiyama, T., and Sasaki, K. (2018). Flight demonstration of a long range onboard doppler lidar. In *Proceedings of the 31st Congress of the International Council of the Aeronautical Sciences*, ICAS 2018–0121.

Japan Transport Safety Board (2015). JTSB digests – case studies and accident analysis –. http://www.mlit.go.jp/jtsb/bunseki-kankoubutu/ jtsbdigests e/jtsbdigests No15/No15 pdf/jtsbdi- 15 all.pdf.

Kikuchi, R. (2017). *Real-Time Prediction of Wind Conditions and Atmospheric Turbulence for Safe and Efficient Aircraft Operation*. PhD thesis, Graduate School of Engineering, Tohoku University.

Matayoshi, N., Iijima, T., Yoshikawa, E., Entzinger, J.O., Uemura, T., Akiyama, T., and Inokuchi, H. (2018). Development and flight demonstration of a new lidar-based onboard turbulence information system. In *Proceedings of the 31st Congress of the International Council of the Aeronautical Sciences*, ICAS 2018–0284.

Misaka, T., Nakabayashi, F.K., Obayashi, S., and Inokuchi, H. (2015). Filtering algorithm of airborne doppler lidar measurements for improved wind estimation. *Transactions of the Japan Society for Aeronautical and Space Sciences*, 58(3), 149–155.

Regan, C.D. and Jutte, C.V. (2012). Survey of applications of active control technology for gust alleviation and new challenges for lighter-weight aircraft. *NASA Technical Memorandum*, NASA-TM-2012-216008.

Sato, M. (2010). Gust alleviation flight controller using robust model predictive control. In *Proceedings of the 18th IFAC Symposium on Automatic Control in Aerospace*.

Sheridan, T.B. (1966). Three models of preview control. *IEEE Transaction on Human Factors in Electronics*, HFE-7(2), 91–102.

Wilcox, J.D. (1956). Isokinetic flow and sampling. *Journal of the Air Pollution Control Association*, 5(4), 226–245.

Wright, J.R. and Cooper, J.E. (2007). *Introduction to Aircraft Aeroelasticity and Loads*. John Wiley & Sons, Ltd, West Sussex PO19 8SQ, England.